

Institute for Astronomy, University of Edinburgh,
Royal Observatory, Blackford Hill, Edinburgh EH9 3HJ,
United Kingdom; Lawrence Berkeley National Laboratory,
Berkeley, CA 94720, U.S.A.;
Jet Propulsion Laboratory, California Institute of Tech-

nology, 4800 Oak Grove Drive, Mail Stop 169-221,
Pasadena, CA 91109, USA; California Institute of Technology,
1200 East California Boulevard, Pasadena, CA
91125, USA; Steward Observatory, 933 North Cherry Avenue,
Tucson, AZ 85721, U.S.A.

THE MID-INFRARED VARIABILITY OF QUASARS: TYPICAL VALUES AND EXTREME OUTLIERS

NICHOLAS P. ROSS¹, AARON MEISNER², DANIEL STERN³, DAVID J. SCHLEGEL², ANDREW DRAKE⁴, MATTHEW GRAHAM⁴,
ET AL., ARJUN DEY⁵, FOR THE DECALS CONSORTIUM.

(Dated: May 8, 2017)
Draft version May 8, 2017

ABSTRACT

We present the mid-infrared light-curves for 248 quasars that show large, >0.5 mag peak-to-peak, variation in either the WISE W1 or W2 (3.4 or 4.6 μm) bands. Our motivation is to quantify and understand the ubiquity and processes involved in luminous AGN obscuration. The quasars are part of the SDSS-I/II or SDSS-III: BOSS Quasar surveys, a superset of over 200,000 objects with at least one epoch of spectroscopy. The IR light curves are from the WISE, NEOWISE and NEOWISE-R missions. Critically we employ new DECALS data, and find objects that were ‘traditional’ blue quasars (and appear so in SDSS imaging) but turn red in color in DECALS, and are often now seen as extended. In particular, we present the $z = 0.378$ quasar SDSS J110057.70-005304.5 as a quasar that is transitioning from a blue continuum sloped object to become a “Changing-Look” quasar – with the prominence of the H β and H γ broad-emission lines being dramatically reduced. What makes J110057 particularly interesting, however, is (by selection) its associated short-term IR variability, and dramatic reddening in the optical continuum during the transition to its non-broad line state. (**TBD!!**) We explore simple models of quasar obscuration, and given the short observed timescales (≈ 7 years in the rest-frame) find it very hard to explain this behavior.

Subject headings: WISE, QSOs

1. INTRODUCTION

The reprocessing of UV/optical photons by micron sized carbonates and silicates around an AGN central engine leads to the prodigious emission of infrared (IR) emission (see Elitzur (2014) for review on AGN infrared emission; Netzer (2015) for a review on the Unified Model of Active Galactic Nuclei, and Draine (2003) for a review on dust).

With the energy released by the accretion of material onto a galactic central engine black hole being comparable to the energy released in nuclear fusion having a full accounting of the bolometric output from a luminous AGN, i.e. a quasar, is a critical part of any contemporary galaxy and AGN model and evolutionary theory (e.g., Rosas-Guevara et al. 2016; Bower et al. 2017; McAlpine et al. 2017; Pillepich et al. 2017). Thus, identifying AGN in the IR, and in particular at $\sim 10\mu\text{m}$ where the AGN contribution to the SED peaks (REFs) is of key interest. Indeed, many studies have explored the utilization of mid-IR (3-30 μm rest) to identify and characterize AGN and quasars (Lacy et al. 2004; Stern et al. 2005; Martínez-Sansigre et al. 2006; Richards et al. 2009; Donley et al. 2012; Stern et al. 2012; Banerji et al. 2013; Assef et al. 2013; Richards et al. 2015; Timlin et al. 2016).

Along with the raw energy output, of further critical importance to understanding in detail the physical pro-

cesses of the AGN, and the potential for “feedback” on the host galaxy, is the time-dependent nature of the obscuring, dusty material. Although this is thought to be a dusty rotating “toroidal” structure on \sim parsec scales, apart from a few very local case studies (e.g. VLT MIR interferometry objects) we are currently very ignorant to the geometry and topology of the AGN IR emitting region.

As such, observing, and characterizing the MIR *light curves* (LCs) of luminous AGN, would garnish major clues into the variable nature of the energy output of the central engine, along with key tests and constraints on the “AGN unified model”.

In this paper, we use the data from the Wide-Field Infrared Survey Explorer (WISE; Wright et al. 2010), and in particular the NEOWISE-R mission (Mainzer et al. 2014; Meisner et al. 2016), combined with the Sloan Digital Sky Survey quasar catalogs (DR7Q; Schneider et al. 2010) and Dark Energy Camera Legacy Survey (DECALS; Lang et al. 2016) to identify 105 quasars (from a sample of 105,000) with large changes, $|\Delta\text{mag}| > 0.5$, in their MIR LCs.

Kozłowski et al. (2010) and use the multi-epoch, mid-infrared Spitzer Deep Wide-Field Survey to investigate the variability of objects in 8.1 deg 2 of the NOAO Deep Wide Field Survey Bootes field. These authors perform a difference image analysis of the four available epochs between 2004 and 2008, over 8.1 deg 2 , focusing on the deeper 3.6 and 4.5 μm bands. Out of 474,179 analyzed sources, 1.1% meet their standard variability selection criteria that the two light curves are strongly correlated and that their joint variance exceeds that for all sources

¹ npross@roe.ac.uk

²

³

⁴

⁵

with the same magnitude by 2σ . Kozłowski et al. (2016) redo this analysis with a longer baseline.

In Section 2 we describe our datasets and methods for finding the MIR variable quasars, including false positive checks. In Section 3 we present our sample and the place the Extreme-IR Changers in context of the general QSO population. In Section 4 we *potentially* say “something” about obscuration rates and draw our conclusions. The (online) Appendix gives the full details of our sample. Because of established conventions, we report SDSS magnitudes on the AB zero-point system (Oke & Gunn 1983; Fukugita et al. 1996), while the WISE magnitudes are calibrated on the Vega system (Wright et al. 2010).

2. DATA

We utilize three large datasets for our investigations: the 5-band, optical Sloan Digital Sky Survey (SDSS; all the usual refs), the 3-band optical Dark Energy Camera Legacy Survey (Lang et al. 2016, DECaLS), and data from the WISE mission. Crucially, data from all three surveys is combined, details of which can be found at legacysurvey.org. We summarize the salient details here.

2.1. Optical Data

2.1.1. SDSS and SDSS-III: BOSS

The SDSS is described in full detail elsewhere (Fukugita et al. 1996; Gunn et al. 1998; York et al. 2000; Hogg et al. 2001; Lupton et al. 2001; Stoughton et al. 2002a; Smith et al. 2002; Pier et al. 2003; Ivezić et al. 2004; Gunn et al. 2006; Tucker et al. 2006; Padmanabhan et al. 2008). The third incarnation of the SDSS, SDSS-III is described in Eisenstein et al. (2011) with the Baryon Oscillation Spectroscopic Survey (BOSS) being detailed in Dawson et al. (2013). The final data release paper from SDSS-III was the Data Release 12 (Alam et al. 2015).

We use the SDSS Seventh Data Release Quasar Catalog (DR7Q; Schneider et al. 2010; Shen et al. 2011) and the SDSS-III Twelve Data Release (DR12Q; Páris et al. 2017). SDSS quasar targets with $i \leq 19.1$ were selected if the colors were consistent with being at redshift $z \lesssim 3$, and $i \leq 20.2$ objects were selected if $z \gtrsim 3$, as outlined in Richards et al. (2002). BOSS quasar targets are selected to a magnitude limit of $g \leq 22.0$ or $r \leq 21.85$, with the primary goal to select quasars in the redshift range $2.2 \leq z \leq 3.5$ as described by Ross et al. (2012, and references therein). In both SDSS and BOSS, quasar targets are also selected if they are matched within $2''$ ($1''$ in the case of BOSS) of an object in the Faint Images of the Radio Sky at Twenty-cm (FIRST) catalog of radio sources (Becker et al. 1995). Both the SDSS DR7Q and BOSS DR12Q include quasars that were selected by algorithms other than the main quasar selections; these sources appear in the catalog due to being targeted by the respective galaxy selections, being a ‘serendipitous’ (Stoughton et al. 2002a) or ‘special’ (Adelman-McCarthy et al. 2006) target in SDSS, or an ‘ancillary’ target in BOSS (Dawson et al. 2013; Alam et al. 2015; SDSS Collaboration et al. 2016).

2.1.2. DECaLS: Dark Energy Camera Legacy Survey

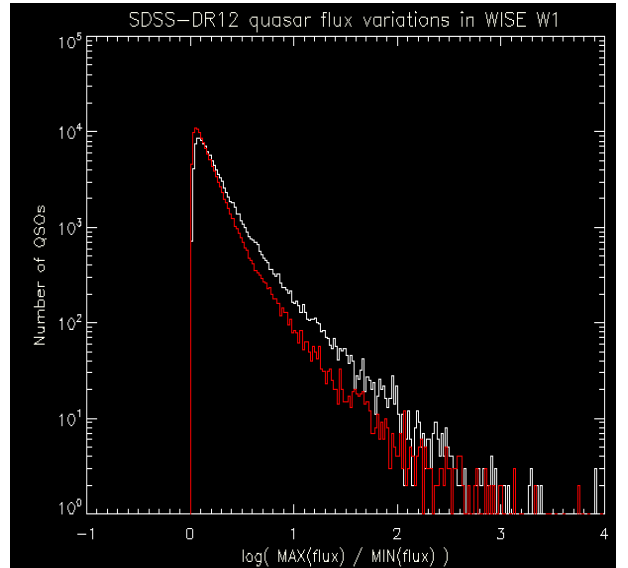


FIG. 1.— The distribution of the maxima and minima flux in $W1$ for the $\sim 240k$ high-confidence quasars in the SDSS-III: BOSS DR12. The red distribution is if one replaces fluxes with a mean flux+measurement error for each observation. Note, since the log is being plotted, the difference between the two lines shows a significant variable population. There are ~ 1000 quasars where the $W1$ flux varies by more than a factor of 2 with a > 5 sigma confidence. Some have a poor χ^2 fits.

The Dark Energy Camera Legacy Survey (DECaLS; Lang et al. 2016) is taking deep 3-band g, r, z imaging over 10,000deg of the Northern Sky that is accessible from the Cerro Tololo International Observatory site. As of writing the DECaLS is ongoing.

2.2. Infrared Data

As noted in Mainzer et al. (2014) and Meisner et al. (2016), after its initial launch, cryogenic mission, and a period of hibernation, the WISE satellite was reactivated, and recommenced surveying the sky in its two shorter wavebands, $W1$ and $W2$. This $W1/W2$ survey is referred to as NEOWISE-Reactivation or NEOWISER.

We directly use the data from Meisner et al. (2016) which employs an adaptation of the unWISE Lang (2014) image coaddition framework.

From the Tractor catalog column descriptions, you will see that DR3 includes sparse WISE $W1/W2$ light curves for every optically detected source (WISE_LC*). These WISE light-curves are measured by forced-photometry of time-resolved unWISE coadds. Currently, in the DECaLS footprint, there are typically four epochs, sometimes five, and very rarely only three. These light curves typically span a ~ 4 -5 year time baseline, ~ 2010 -2014.

The distribution of the maxima and minima flux in $W1$ for the $\sim 240k$ high-confidence quasars in the SDSS-III: BOSS DR12 is given in Figure 1.

2.3. “False Positive Checks”

Figure 2 is the distribution of $(\text{max-min})/\text{error}$ in the MIR fluxes. (Should also be looking at the SDSS stars as a control sample). The WISE magnitude range for those stars will be quite different, though, since they have the same optical magnitude range but are fainter in WISE.

$W1$ and $W2$ lightcurves for $\sim 200,000$ SDSS spectroscopic quasars were extracted from Data Release 3 (DR3)

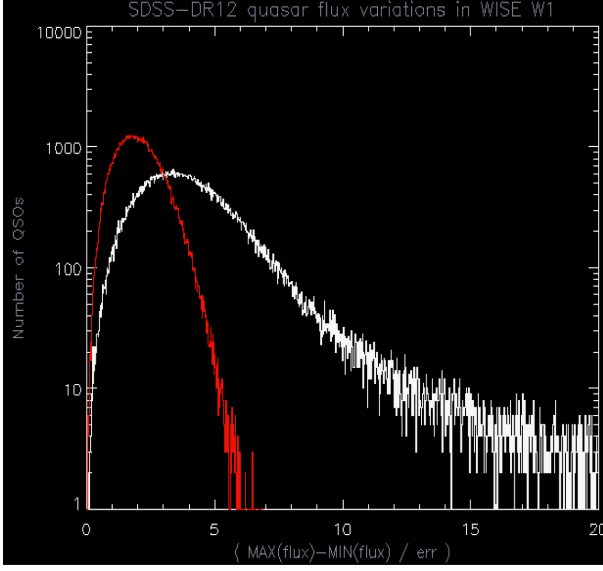


FIG. 2.— Here, “err” is the quadrature sum of the errors at the minimum and maximum fluxes. The red histogram is the expected distribution if these objects had no variability, and the errors were normally-distributed for each of the epochs. This shows that ~6,000 quasars are $> 10\sigma$ detections of variability in W1.

of the Dark Energy Camera Legacy Survey (DECaLS). These light curves span from the beginning of the WISE mission (2010 January) through the first-year of NEOWISER operations (2014 December). In detail, the W1/W2 light curves are obtained by performing forced photometry at the locations of DECam-detected optical sources. This forced photometry is performed on time-resolved unWISE coadds, each of which represents a stack with depth of coverage ~ 12 exposures. A given sky location is observed by WISE for ~ 1 day once every six months, which means that our forced photometry light curves typically have four coadd epochs available. Coadd epochs of a given object are separated by a minimum of six months and a maximum of four years. Our coaddition removes the possibility of probing variability on $\lesssim 1$ day time scales, but it allows us to push ~ 1.4 magnitudes deeper than individual exposures while removing virtually all single-exposure artifacts (e.g. cosmic rays and satellites).

$\sim 30,000$ of the SDSS quasars with such W1/W2 lightcurves available are “IR-bright”, in the sense that they are above both the W1 and W2 single exposure thresholds and therefore detected at very high significance in our coadds. For this ensemble of objects, the typical variation in each quasar’s measured (W1-W2) color is 0.06 magnitudes, which includes statistical and systematic errors expected to contribute variations at the few hundredths of a mag level. The typical measured single-band scatter is 0.07 magnitudes in each of W1 and W2. A full characterization of the typical mid-IR quasar variability will be presented separately (Ross et al., in preparation).

We undertook a search for extreme outliers relative to these trends. Specifically, we selected objects with the following characteristics.

- Monotonic variation in both W1 and W2.
- W1 versus W2 *flux* correlation coefficient > 0.9 .

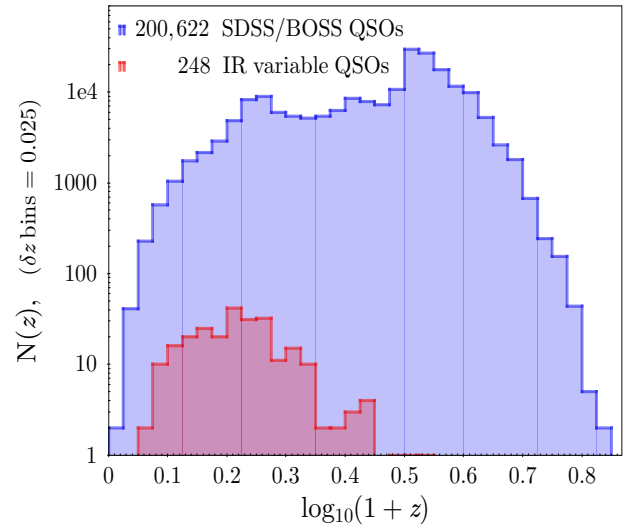


FIG. 3.— The the variations in ($W1 - W2$) color using $\sim 37,500$ data points from ~ 9000 bright quasars. Overplotted is a Gaussian distribution, centered at -3.8 mmag and with standard deviation of 0.06 mags (with a fit-by-eye :-).

- > 0.5 mag peak-to-peak variation in either W1 or W2.

This yielded a sample of 248 sources. 31 of these are assumed to be blazars due to the presence of FIRST radio counterparts. Another 22 are outside of the FIRST footprint, leaving 195 quasars in our IR-variable sample. We randomly selected five of these objects for follow-up spectroscopy with Palomar DBSP on the night of 30 January 2017. WISE J1052+1519, one of these five, faded by 0.75 (0.9) mags in W1 (W2), and thus became 0.15 mags bluer in ($W1 - W2$), making it a significant outlier in both single-band and IR color variability.

A link to the key properties of our sample can be found here: `qso_pages_v01` and the links to the catalogs are given here: `dr3_wise_lc_sample.fits.gz` and here: `dr3_wise_lc_sample.fits.gz`. The first catalog has 248 rows, which are the selected highly IR-variable sample of objects. The second catalog is the full 200 622 quasar sample quasars that have “good” WISE light curves available in DECaLS DR3. In each file, there are 3 extensions: ex = 0 – WISE light curve summary metrics; ex = 1 – DECaLS DR3 Tractor data for each object; ex = 2 – SDSS data for each object.

3. RESULTS: GENERAL POPULATION

Starting from the $\approx 200,000$ object parent quasar sample, and employing the selections as described above, we generate a catalog of 248 objects. Some general properties include:

- The redshift distribution of the IR-variable sample of objects being at generally lower redshift than the parent sample, but extending to relatively high- z - see Figure 3;
- 221 (89%) of the sample have falling IR lightcurves.
- The extremely IR variable QSOs generally have the same optical colors as the parent population, see Figures 6 and 7.

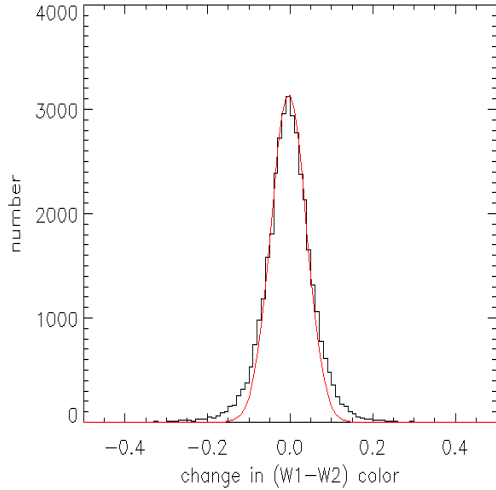


FIG. 4.— The variations in $(W_1 - W_2)$ color using $\sim 37,500$ data points from ~ 9000 bright quasars. Overplotted is a Gaussian distribution, centered at -3.8 mmag and with standard deviation of 0.06 mags (with a fit-by-eye ;-).

The $N(z)$ redshift distributions are shown in Figure 3 with the parent sample the blue histogram and the IR-variable sample the red histogram.

Lorem ipsum dolor sit amet, consectetur adipiscing elit. Aliquam porta sodales est, vel cursus risus porta non. Vivamus vel pretium velit. Sed fringilla suscipit felis, nec iaculis lacus convallis ac. Fusce pellentesque condimentum dolor, quis vehicula tortor hendrerit sed. Class aptent taciti sociosqu ad litora torquent per conubia nostra, per inceptos himenaeos. Etiam interdum tristique diam eu blandit. Donec in lacinia libero.

3.1. Color Changes

Figure 4 shows the variations in the $(W_1 - W_2)$ color, which is pretty narrow. Overplotted is a Gaussian distribution, centered at -3.8 mmag and with standard deviation of 0.06 mags.

This histogram includes $\sim 37,500$ data points from ~ 9000 bright quasars, that is, brighter than single-exposure detection limit in both W_1 and W_2 . *NPR: It'd be very most awesome if we could show a $W_1W_2W_3$ RGB image of a quasar changing color!!!*

Figure 5 has the same data as Fig 4, now in a scatterplot of $\Delta(W_1)$ versus $\Delta(W_2)$. There is clearly some variation, and it is well-correlated between W_1 and W_2 . The red line is $x = y$. (I would guess this is real variation, but I'm still a little bit scared that you could have e.g. correlated background level issues in the coadds that imprint onto the fluxes.)

Etiam mollis viverra nisi eget aliquet. Aliquam erat volutpat. Vivamus tristique, nisl eu malesuada semper, libero tortor convallis elit, a scelerisque orci nisi lacinia turpis. In lacinia ultrices volutpat. Proin ultrices luctus tellus, in placerat eros tincidunt id. Ut varius iaculis quam in consequat. Nulla nec orci est, sit amet pellentesque nisl. Mauris non cursus lectus. Praesent placerat leo vel erat gravida lacinia. Donec vehicula consectetur lectus vitae luctus. Praesent nisl justo, laoreet elementum facilisis vel, tristique ac enim. Etiam vel quam ut quam eleifend tincidunt. Suspendisse sit amet eros vel

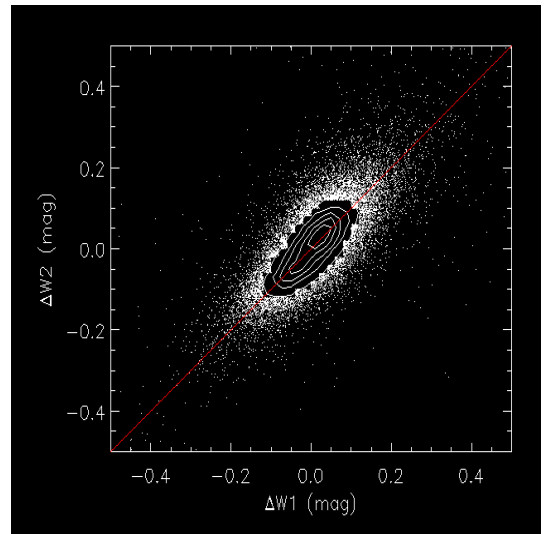


FIG. 5.— The variations in $(W_1 - W_2)$ color using $\sim 37,500$ data points from ~ 9000 bright quasars. Overplotted is a Gaussian distribution, centered at -3.8 mmag and with standard deviation of 0.06 mags.

elit ullamcorper laoreet. Etiam venenatis sodales turpis, nec lacinia ligula hendrerit nec. Nam eu vulputate purus. Quisque facilisis congue metus, sed imperdiet lorem rhoncus sit amet.

3.2. Changes in color: One IR Variable population or two?

Turpis tincidunt quam consectetur non suscipit telus placerat. Etiam sit amet justo condimentum sem scelerisque pharetra. Nullam sit amet neque eget quam tempor consectetur vel vitae massa. Nunc porttitor, quam in tempor pharetra, leo libero eleifend mi, ac ornare nibh eros vel purus. Pellentesque lobortis enim metus.

4. RESULTS: INDIVIDUAL OBJECTS

Having placed the IR variable quasars in context with their parent population, we now turn our attention to objects with particularly interesting features, using due to having repeat spectroscopy available.

The object SDSS J105203.55+151929.4 is one of the IR variable sample and is the first CLQ to be discovered through its IR properties. Stern et al. (2017, in prep.) has a detailed study of that object.

In this paper, we will turn our focus to another very interesting object, SDSS J110057.71-005304.5.

4.1. SDSS J110057.71-005304.5

Figures ?? presents the IR NEOWISER light curve for J110057, and ?? the IR finding charts.

SDSS J110057.71-005304.5, hereafter J110057, was discovered by the Sloan Digital Sky Survey in 2000. J110057 was imaged in Run 756 (which makes up Stripe 10), and satisfied a number of spectroscopic targeting flags¹ making it a quasar target. A spectrum was obtained on MJD 51908, on Plate 277, Fiber 212, and the spectrum of a $z = 0.378 \pm 0.00003$ was

¹ SERENDIP_BLUE, ROSAT_D, ROSAT_C, ROSAT_B, QSO_SKIRT, ROSAT_A, see Stoughton et al. (2002b) and Richards et al. (2002) for flag descriptions.

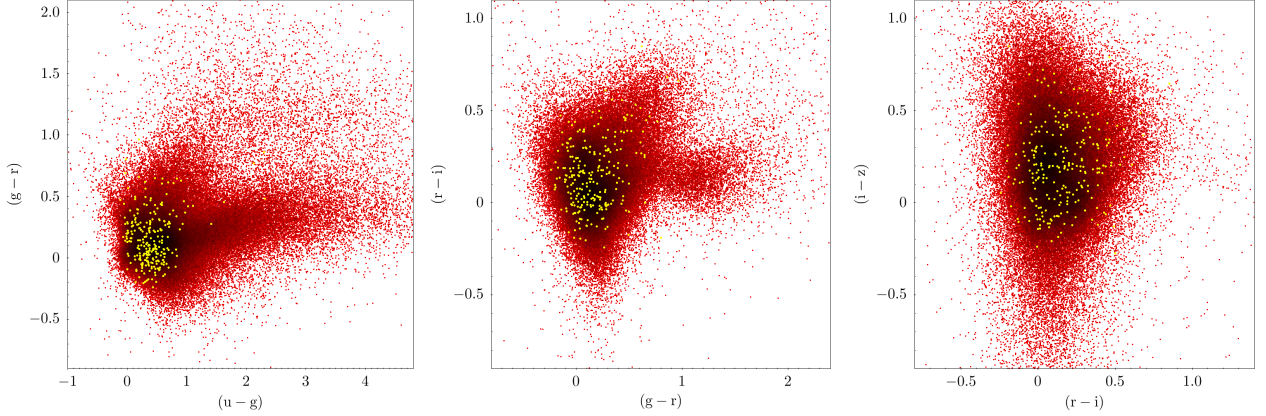


FIG. 6.— The *ugriz* color-color plots for the full 200k super-sample (red points) and the 248 extreme IR variables (yellow dots).

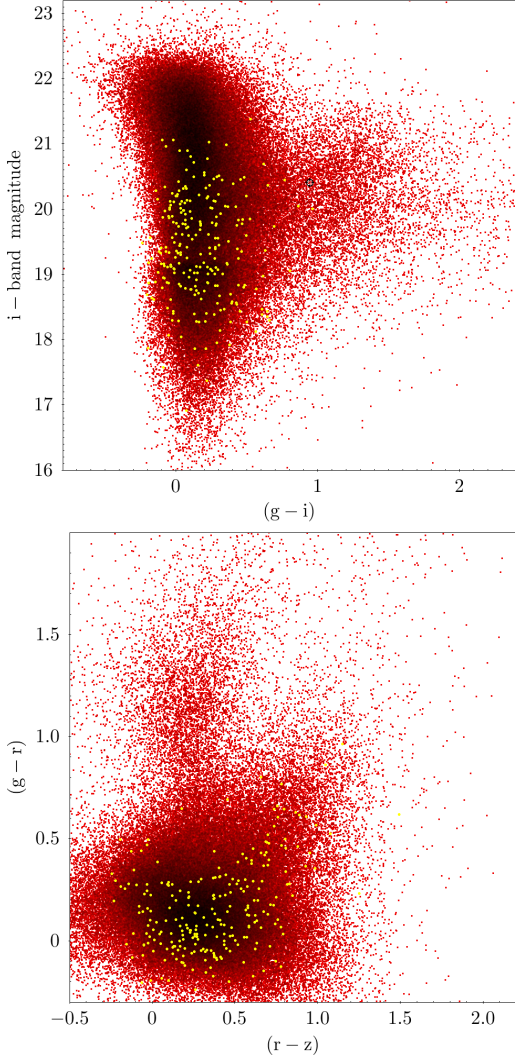


FIG. 7.— The color-mag and *grz* color-color plots for the full 200k super-sample (red points) and the 248 extreme IR variables (yellow).

In the DECaLS, the DECaLS brick containing J110057.71-005304.5. There are 8, 3 and 9 exposures in the *g*-, *r*- and *z*-band respectively. $56707.146 \leq g_{\text{MJD}} \leq 56727.201$; $56367.091 \leq r_{\text{MJD}} \leq 56367.230$; $56383.159 \leq z_{\text{MJD}} \leq 57398.350$.

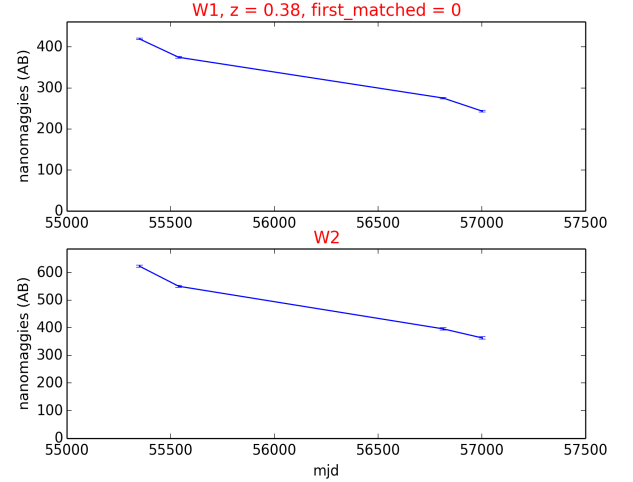


FIG. 8.— WISE infrared light-curve for J110057.

As can be seen, the *g*- and *r*-band observations have fairly limited time spans, and are separated by roughly a year. The *z*-band observations span almost 3 years. The DESI imaging brick name is 1651m010.

Second epoch spectrum is from BOSS and has a dramatic downturn at $\lesssim 4300\text{\AA}$.

A third epoch spectrum was obtained from the Palomar 5m telescope using the DBSP instrument. Two exposures of 600s+300s were taken in good conditions. Feature to note include: the continuum straddling MgII being blue in the 2017 spectrum, as it was for the SDSS spectrum in 2000, as opposed to red, as it was for the BOSS spectrum in 2010.

LOREM IPSUM DOLOR SIT AMET, CONSECTETUR ADIPISCING ELIT. ALIQUAM PORTA SODALES EST, VEL CURSUS RISUS PORTA NON. VIVAMUS VEL PRETIUM VELIT. SED FRINGILLA SUSCIPIT FELIS, NEC IACULIS LACUS CONVALLIS AC. FUSCE PELLentesQUE CONDIMENTUM DOLOR, QUIS VEHICULA TORTOR HENDERIT SED. CLASS APTEnt TACITI SOCIOSQU AD LITORA TORQUENT PER CONUBIA NOSTRA, PER INCEPTOS HİMENAEOS. ETIAM INTERDUM TRISTIQUE DIAM EU BLANDIT. DONEC IN LACINIA LIBERO.

Sed elit massa, eleifend non sodales a, commodo ut felis. Sed id pretium felis. Vestibulum et turpis vitae quam aliquam convallis. Sed id ligula eu nulla ultrices tempus. Phasellus mattis erat quis metus dignissim malesuada. Nulla tincidunt quam volutpat nibh facilisis euismod. Cras vel auctor neque. Nam quis diam risus.

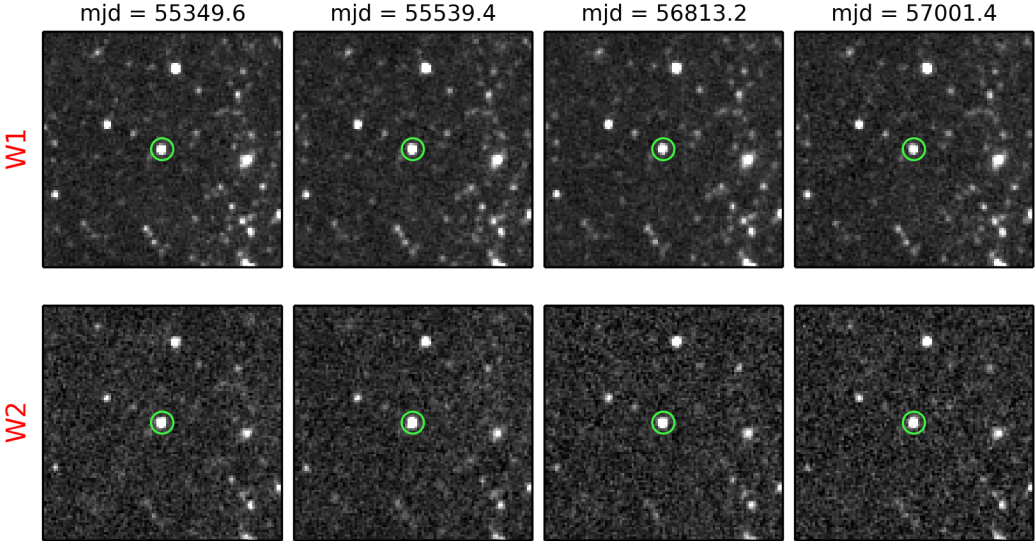


FIG. 9.— WISE thumbnail images for J110057.

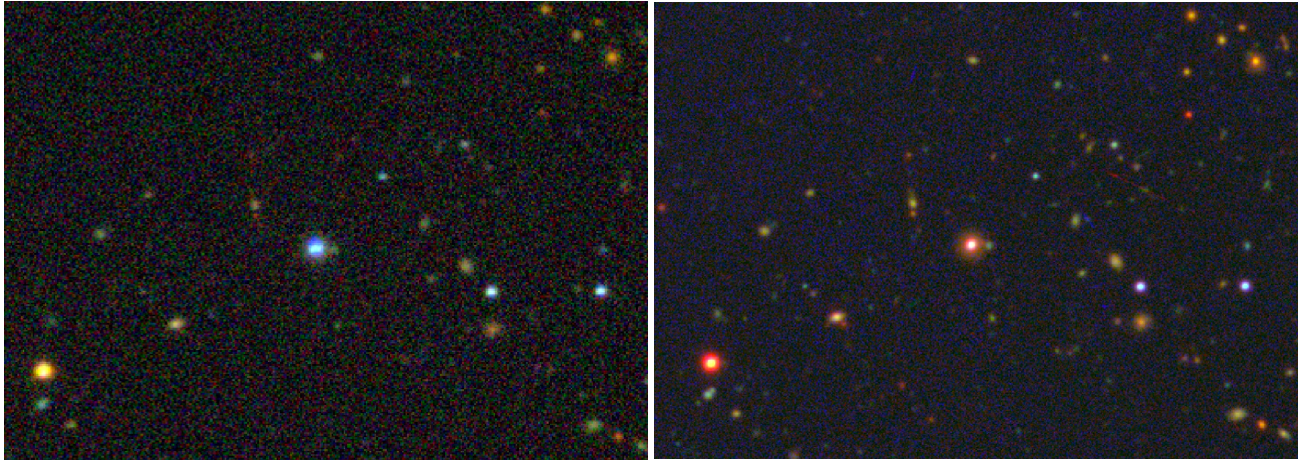


FIG. 10.— The SDSS (*left*) and DECaLS (*right*) image of SDSS J110057.71-005304.5 (*center*).

Nunc semper quam et leo interdum vulputate eu quis magna. Sed nec arcu at orci egestas convallis. Aenean quam velit, aliquam vitae viverra in, elementum vel elit. Nunc suscipit aliquet sapien a suscipit. Cras nulla ipsum, posuere eu fringilla sit amet, dapibus ultricies nulla. Nullam eu augue id purus mollis dignissim sed et libero. Phasellus eget justo sed neque pellentesque egestas nec id arcu. Donec facilisis pulvinar sapien et fringilla. Suspendisse vestibulum rhoncus sapien id laoreet. Morbi et orci vitae tortor imperdiet imperdiet. In hac habitasse platea dictumst. Vivamus vel neque id mi ultrices tristique. Integer quam libero, ornare vel gravida in, feugiat a ante. Nam dapibus, tellus vitae pellentesque cursus, dui nisl egestas augue, non fermentum nisl est nec nisi. Vestibulum nec mi justo, eget dapibus velit.

5. DISCUSSION

In the above sections, we placed the variable IR quasar sample in context to the parent quasar population. We also discussed SDSS J110057.71-005304.5 as a standout solo object. In this section, we model the observed prop-

erties of J110057 to understand its central engine properties. We then attempt to link the IR Variability to the Changing Look phenomena in general.

5.1. Modeling the IR light-curves and the optical spectra of J110057

Nunc semper quam et leo interdum vulputate eu quis magna. Sed nec arcu at orci egestas convallis. Aenean quam velit, aliquam vitae viverra in, elementum vel elit. Nunc suscipit aliquet sapien a suscipit. Cras nulla ipsum, posuere eu fringilla sit amet, dapibus ultricies nulla. Nullam eu augue id purus mollis dignissim sed et libero. Phasellus eget justo sed neque pellentesque egestas nec id arcu. Donec facilisis pulvinar sapien et fringilla. Suspendisse vestibulum rhoncus sapien id laoreet. Morbi et orci vitae tortor imperdiet imperdiet. In hac habitasse platea dictumst. Vivamus vel neque id mi ultrices tristique. Integer quam libero, ornare vel gravida in, feugiat a ante. Nam dapibus, tellus vitae pellentesque cursus, dui nisl egestas augue, non fermentum nisl est nec nisi. Vestibulum nec mi justo, eget dapibus velit.

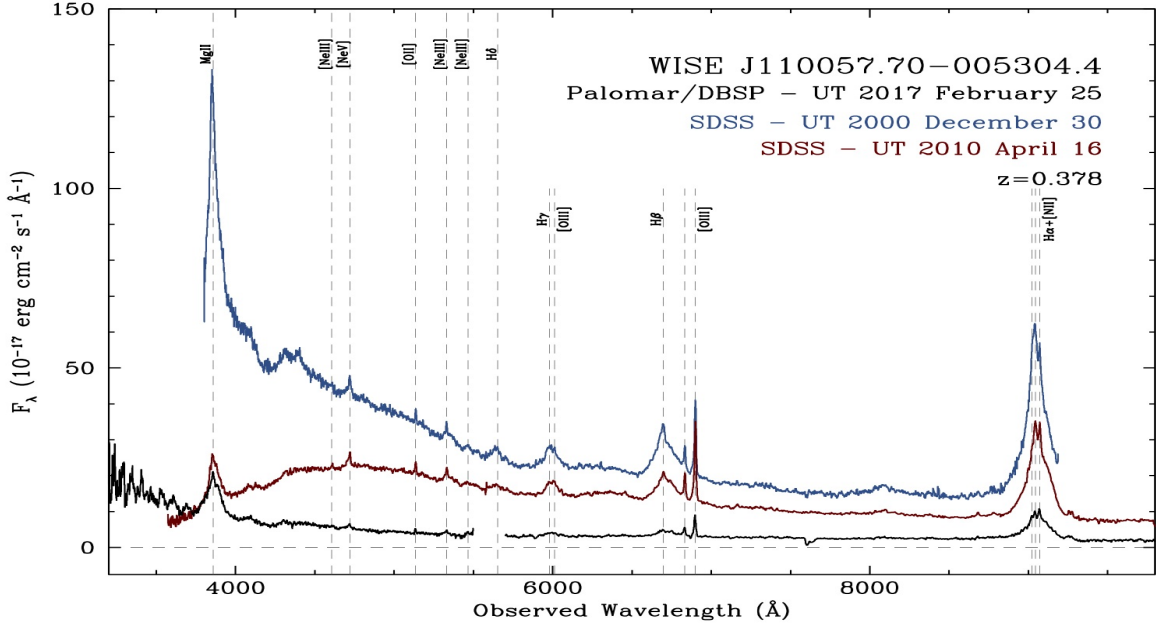
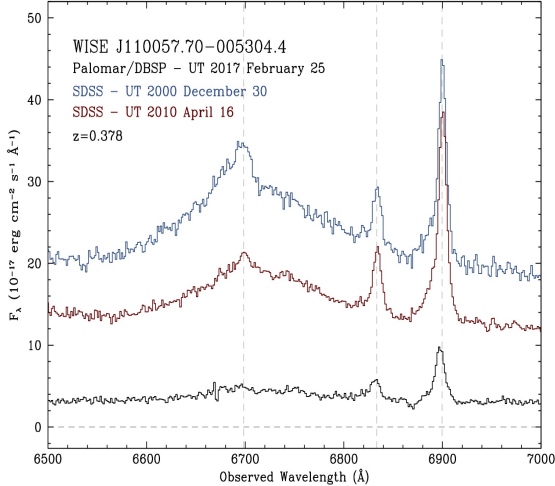


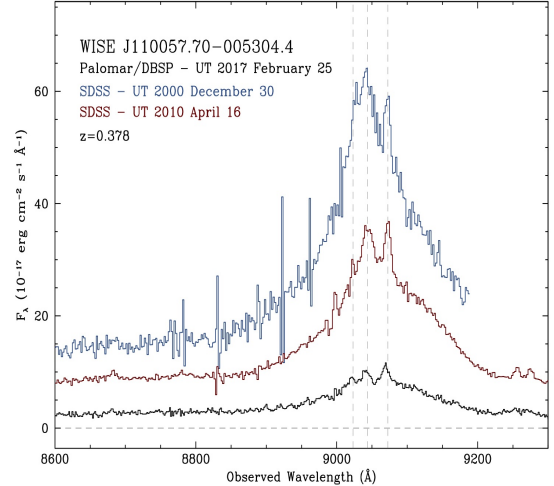
FIG. 11.—

FIG. 12.— SDSS J110057.71-005304.5 H β zoom-in.

5.2. Linking IR Variability to the Changing Look phenomena

Sed sed ipsum diam. In risus tortor, sagittis eu auctor in, varius in dui. Mauris a nunc ut ligula ullamcorper tincidunt. Nunc aliquam eros ac risus pellentesque aliquam. Phasellus augue velit, varius at porttitor sit amet, pretium eget felis. Ut mollis tellus elementum magna porttitor rutrum. Etiam blandit leo eget est consectetur imperdiet. Quisque et diam nec orci vulputate varius vitae id sapien.

Donec elit tortor, scelerisque ac molestie id, hendrerit sit amet ipsum. Maecenas non tempus sem. Pellentesque ut enim velit, eu sagittis elit. Nulla in elementum erat.

FIG. 13.— SDSS J110057.71-005304.5 H α zoom-in.

In dictum arcu at nisi porttitor commodo. Donec felis felis, elementum sit amet ultrices ac, interdum nec ante. Nullam eget faucibus lectus. Donec vitae eros sapien, et faucibus ligula. Aenean pharetra viverra fermentum.

6. DISCUSSION AND CONCLUSIONS

Sed non felis iaculis dui iaculis mattis facilisis ullamcorper ipsum. Donec erat nunc, consectetur et ornare in, egestas vitae mauris. Praesent suscipit rutrum purus, in interdum tellus euismod sit amet. Nulla facilisi. Etiam nisl ligula, vehicula at fringilla et, sagittis eu odio.

Our conclusions are thus:

- Hendrerit pretium commodo. Cras dapibus

SDSSJ	RA	DEC	Z	PLATE	FIBER	MJD	PEARSON_R	BEST_FLUX	W1	BEST_F
000920.76+033021.7	2.33654086687	3.50603303134	0.432505905628	14294	190	53800	0.999489	72,078	94.1	
001053.44+231604.9	2.72267621623	23.2680334774	0.752258002758	16380	202	53800	0.999483	12,077	127.1	
001130.39+005751.8	2.87665180272	0.964415750637	1.49	14275	946	55478	0.999884	132.038	219.1	
001238.49+230328.8	3.16041434409	23.0580121564	0.872348427773	6881	359	56540	0.997853	43.7786	63.1	
001254.25+193707.9	3.22604854198	19.6188883647	0.503228604794	6174	732	56243	0.941408	37.1137	52.1	
001539.99+170040.5	3.91663820339	17.0112615148	1.7200088501	6111	100	56270	0.988381	38.0622	63.1	
001702.88+250559.6	4.26201771268	25.09990315	0.243872866035	6279	660	56243	0.999826	92.0064	120.1	
001744.44+253123.6	4.43518860333	25.523231208	0.758191466331	6279	678	56243	0.970858	52.0593	44.1	
002125.18+231025.1	5.35494705482	23.1736602346	0.815230727196	6882	394	56541	0.996137	49.8901	60.1	
002810.91+262510.7	7.04547508037	26.4196389292	0.862826228142	6281	743	56295	0.947475	32.2795	46.1	
002917.29+024619.8	7.32205987295	2.77217878694	0.726760387421	6221	142	56243	0.999005	85.1136	107.1	
003625.84+011258.4	9.10767697614	1.21622940345	0.86627805233	6221	142	56243	0.999815	28.0893	47.1	
003859.67-034000.7	9.74864452147	-3.66688077687	0.865895032883	6221	142	56243	0.999815	53.541	102.1	
004530.42+125403.3	11.3767895588	12.9009196152	0.655647099018	6202	156	56266	0.991671	51.9636	92.1	
004653.63+053406.8	11.7234836086	5.56855949673	0.790611922741	6203	156	56266	0.999815	78.4327	74.1	
010044.21-040810.9	15.1842109756	-4.13638255411	0.566544234753	7043	764	56576	0.970251	93.7984	104.1	
011118.69+235808.8	17.8278966604	23.9691236157	0.90282279253	7043	764	56576	0.970251	47.7996	85.1	
012141.59+114950.4	20.42330313661	11.8306723861	0.5713153481	7043	764	56576	0.970251	89.1521	120.1	
021104.17-045325.0	32.7674053995	-4.89030505937	0.525170624256	7228	981	56660	0.974047	58.9339	78.1	
021740.47-035029.3	34.4186466932	-3.8414779352	0.105192315578	7257	946	56662	0.907251	31.4279	66.1	
024026.72+014255.9	40.111353931	1.71552955684	0.842329204082	7261	300	55503	0.914861	31.1816	67.1	
083750.72+063633.6	129.46136597	6.60934044369	0.634521722994	7261	300	55503	0.914861	19.0226	75.1	
083859.40+171510.5	129.747501013	17.2529354994	0.696680605412	7261	300	55503	0.914861	52.9636	59.1	
084118.14+015406.6	130.325624207	1.90183929163	0.426525354385	7261	300	55503	0.914861	110.361	64.1	
085036.06+040810.4	132.650290161	4.13624621005	0.455819457769	7261	300	55503	0.914861	229.2295	15.1	
090343.63+102305.3	135.931804511	10.3848111529	0.634052336216	7261	300	55503	0.914861	41.4461	43.1	
090807.72+120010.3	137.032171668	12.0028850696	0.90961533784	7261	300	55503	0.914861	27.3048	42.1	
092118.48+295735.2	140.327038653	29.9597852233	0.761953532698	7261	300	55503	0.914861	50.6972	99.1	
092750.78+200303.0	141.961601946	20.0508375164	0.941165745258	7261	300	55503	0.914861	31.4169	42.1	
093148.13+234837.0	142.950567427	23.8103001882	0.891499459743	7261	300	55503	0.914861	70.1	70.1	
094554.40-002026.2	146.476672377	-0.340617322862	0.6825953722	7261	300	55503	0.914861	1.5159	51.1	
095538.30+241321.6	148.909599109	24.2226903891	0.800511419778	7261	300	55503	0.914861	15.1	71.1	
100818.54+264434.9	152.077280407	26.7430444161	0.734007418156	7261	300	55503	0.914861	69.128	69.1	
101216.39+231214.6	153.068293641	23.2040630428	0.74982595437	7261	300	55503	0.914861	20.1	12.1	
101337.44+302107.9	153.406016464	30.3522165184	2.0	7261	300	55503	0.914861	51.1	51.1	
101403.18+251608.6	153.513277422	25.2690779765	0.2	7261	300	55503	0.914861	71.1	71.1	
102136.98+004613.4	155.404095536	0.6552490592	0.1	7261	300	55503	0.914861	98.1	98.1	
102221.32+102623.7	155.588484588	10.4399373421	0.6552490592	7261	300	55503	0.914861	33.3	33.3	
102357.34+223512.6	155.988939085	22.5868549001	1.0945917303	7261	300	55503	0.914861	49.1	49.1	
102639.42+274931.5	156.6642744191	27.8524297012	0.65551906824	7261	300	55503	0.914861	58.1	58.1	
102700.25+290938.2	156.751082432	29.1606259158	0.51579207160	7261	300	55503	0.914861	25.8011	20.1	
102834.03-023659.6	157.141820386	-2.6165715345	0.4702049798	7261	300	55503	0.914861	40.4	40.4	
103931.57+231922.1	159.881574851	23.32284264525	0.159	7261	300	55503	0.914861	88.821	88.8	
104355.02+232200.4	160.97926975	23.3667782211	0.888	7261	300	55503	0.914861	64.3281	83.1	
110106.26+040747.1	165.276120081	4.12976474608	0.721132516861	7261	300	55503	0.914861	108.1	108.1	
110305.62+225730.7	165.773422765	22.9585550062	1.0945917303	7261	300	55503	0.914861	71.1	71.1	
110427.76+225945.4	166.115696692	22.995968883	0.65551906824	7261	300	55503	0.914861	156.037	156.037	
110514.15+233336.7	166.308969702	32.5602210987	1.1013944191	7261	300	55503	0.914861	15.3864	15.3864	
11146.89+331140.3	168.528495822	33.1945438871	0.820761263371	7261	300	55503	0.914861	20.1715	20.1715	
111428.59+280101.0	168.619126882	28.0169704405	0.519690215888	7261	300	55503	0.914861	84.8421	84.8421	
111516.32+252153.5	168.818002534	25.3648798047	0.3710970878N	7261	300	55503	0.914861	178.1781	178.1781	
111624.30+164056.7	169.101273928	16.6824180729	0.79071313128	7261	300	55503	0.914861	36.9063	56.561	
111947.60+233553.9	169.94836484	23.5943244949	0.146632447839	7261	300	55503	0.914861	15.4275	20.2073	
112402.70+233645.8	171.011259687	23.612737008	1.553	7261	300	55503	0.914861	19.194	21.2111	
112504.41+233634.6	171.268409391	23.6096192086	0.41203638974	7261	300	55503	0.914861	21.2111	21.2111	
113642.64+210434.6	174.177686967	21.0762824157	0.649329125841	7261	300	55503	0.914861	45.4584	45.4584	
114207.51+214508.1	175.531296967	21.752263778	0.654892623424	7261	300	55503	0.914861	65.651	65.651	
114701.59+264404.3	176.756564476	26.7345411593	0.436697334051	7261	300	55503	0.914861	98.981	98.981	
114747.32+242445.7	176.947172998	24.4126971279	0.52284764252	7261	300	55503	0.914861	188.1839	188.1839	
114748.03+273928.9	176.950146949	27.6580538672	0.841322779640	7261	300	55503	0.914861	40.4	40.4	
115110.95+322949.2	177.795634789	32.4970257281	0.614662408820	7261	300	55503	0.914861	48.4827	48.4827	
115400.90+235043.0	178.503784663	23.8452930578	0.826456069494	7261	300	55503	0.914861	58.582	58.582	
120729.36-003214.3	181.872349765	-0.537323608276	0.3992190033	7261	300	55503	0.914861	114.1137	114.1137	
120951.76+181006.8	182.465668737	18.1685683484	0.844826877117	7261	300	55503	0.914861	235.26	333.3	
121307.16+221627.8	183.279859553	22.2744110502	0.8158909784	7261	300	55503	0.914861	66.661	66.661	
121949.78+245430.6	184.957453211	24.9085144597	0.729886353016	7261	300	55503	0.914861	37.377	37.377	
122205.53+130831.2	185.5523050635	13.1420184736	0.873387873173	7261	300	55503	0.914861	64.644	64.644	
123100.81+160834.6	187.753395638	16.1429535635	0.191316137387	7261	300	55503	0.914861	377.377	377.377	
123725.24+114158.5	189.355190861	11.699593202	0.765600681058	7261	300	55503	0.914861	11.6993	23.33	
124652.20+323722.6	191.717529805	32.622951888	0.95	7261	300	55503	0.914861	73.73	73.73	
125032.57+021632.1	192.635731815	2.27559908424	Institutions of the	7261	300	55503	0.914861	168.168	168.168	
125757.23+322929.2	194.488471576	32.4914701889	the University of Arizona,	7261	300	55503	0.914861	123.123	123.123	
130055.53+040551.8	195.231415013	4.09774057575	the Brazilian Participation	7261	300	55503	0.914861	238.238	238.238	
131401.23+301439.0	198.505155287	30.2441742658	the University of Cambridge,	7261	300	55503	0.914861	528.528	528.528	
132527.12+074925.4	201.363021305	7.8237374883	Collaboration including	7261	300	55503	0.914861	38.38	38.38	
133157.27+221206.4	202.98863151	22.3517984161	the National Science Foundation,	7261	300	55503	0.914861	61.619	61.619	
134508.04-000526.6	206.283516426	-0.090733530434	the Department of Energy,	7261	300	55503	0.914861	100.100	100.100	
141339.60+252029.5	213.415023121	25.3415461302	The Instituto de Astronómica de Canarias,	726						

Planck Institute for Astrophysics, New Mexico State University, New York University, Ohio State University, Pennsylvania State University, University of Portsmouth, Princeton University, the Spanish Participation Group, University of Tokyo, University of Utah, Vanderbilt University, University of Virginia, University of Washington, and Yale University.

Facilities: SDSS, BOSS, WISE, CTIO Blanco+DECam

APPENDIX

TECHNICAL DETAILS

All good papers have to have an Appendix.

SDSS Info	Description	Example
SDSSJ	SDSS object name	000920.76+033021.7
RA	SDSS object R.A. (J2000)	002.33654086687
DEC	SDSS object Decl.(J2000)	+003.50603303134
Z	SDSS (pipeline) redshift	0.432505905628
MJD	Modified Julian Date	55806
FIBER	Fiber number	0196
PLATE	Plate number	4297
U_FLUX	u-band flux	10.1695
G_FLUX	g-band flux	13.8142
R_FLUX	r-band flux	14.1181
I_FLUX	i-band flux	16.7872
Z_FLUX	z-band flux	21.7649
DR	Data Release number	12
FIRST_MATCHED	Matched in FIRST radio survey?	0
<hr/>		
WISE LC Metrics	Description	Example
MEAN_SNR_W1	Mean Signal-to-noise, W1	38.8656
MEAN_SNR_W2	Mean Signal-to-noise, W2	22.8657
PEARSON_R	Pearson correlation coefficient	0.999489
N_EPOCH	number of WISE epochs	4
NBAD_W1	Quality flag for epochs??	0
NBAD_W2	Quality flag for epochs??	0
MONO_W1	a	1
MONO_W2	b	1
BEST_FLUX_W1	c	72.078
BEST_FLUX_W2	d	94.7315
CHI2_W1	e	170.705
CHI2_W2	f	88.7313
RCHI2_W1	g	56.9016
RCHI2_W2	h	29.5771
FLUX_MIN_W1	i	56.8723
FLUX_MAX_W1	j	86.1033
FLUX_MIN_W2	k	69.1232
FLUX_MAX_W2	l	114.478
MAG_RANGE_W1	m	0.450297
MAG_RANGE_W2	n	0.547747
GOOD_EPOCH_MASK o	[1 1 1 1 0]	
RISING_W1	p	0
FALLING_W1	q	1
RISING_W2	r	0
FALLING_W2	s	1
COADD_ID	t	0030p030
X_COADD	u	1923.45
Y_COADD	v	1648.51
<hr/>		
Name	Description	Example
BRICKID	Brick ID [1,662174]	
BRICKNAME	Name of brick, near RA=112.6, Dec=+22.2	eg "1126p222"
OBJID	Catalog object number within this brick;	
BRICK_PRIMARY	a unique identifier hash is BRICKID,OBJID;	
BLOB	True if the object is within the brick boundary	
NINBLOB	Blend family;	contiguously numbered from 0
TYCHO2INBLOB	Number of sources in this BLOB	
TYPE	Is there a Tycho-2 (very bright) star in this blob?	
RA	Morphological model	
RA_IVAR	Right ascension at epoch J2000	
DEC	Inverse variance of RA	
DEC_IVAR	Declination at epoch J2000	
BX	Inverse variance of DEC (no cos term!)	
BY	X position of coordinates in brick image stack	
	Y position) of coordinates in brick image stack	

SPECTROPHOTOMETRY FOR CHANGING LOOK QSO 3836/55302-258

All really good papers have more than one Appendix.

REFERENCES

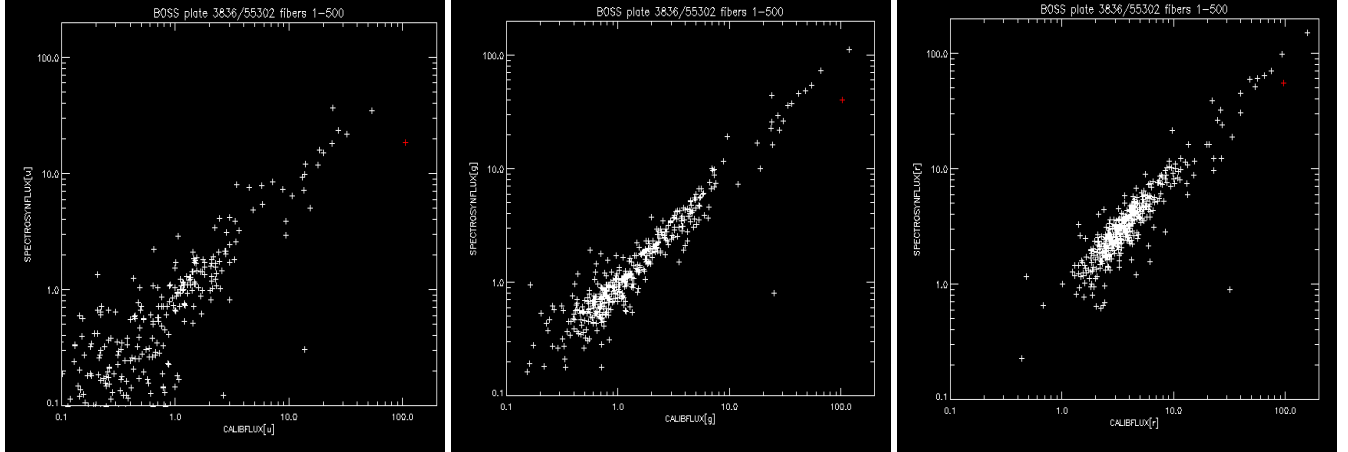


FIG. 14.— The spectrophotometry checks for Changing Look QSO SDSS J110057. From left to right, the u , g and r bands. Along the x -axis is a measurement of the “calibration flux” photometric value which is an estimate of the flux within a 2 arcsecond aperture, and which is the PSF flux value for point objects (stars). On the y -axis is the spectrophotometric flux values. For the SDSS u , g and r -bands from left to right. J110057 is the red point, and is clearly off the general trends for the 500 objects on this half-plate for one the BOSS spectrographs, but is close to the trend in r -band strongly suggesting the variations observed in the BOSS spectra are real.

- Assef R. J., et al., 2013, ApJ, 772, 26
 Banerji M., McMahon R. G., Hewett P. C., Gonzalez-Solares E., Koposov S. E., 2013, MNRAS, 429, L55
 Becker R. H., White R. L., Helfand D. J., 1995, ApJ, 450, 559
 Bower R. G., Schaye J., Frenk C. S., Theuns T., Schaller M., Crain R. A., McAlpine S., 2017, MNRAS, 465, 32
 Dawson K., et al., 2013, AJ, 145, 10
 Donley J. L., et al., 2012, ApJ, 748, 142
 Draine B. T., 2003, ARA&A, 41, 241
 Eisenstein D. J., Weinberg D. H., et al., 2011, AJ, 142, 72
 Elitzur M., 2014, MNRAS, 438, 3340
 Fukugita M., Ichikawa T., Gunn J. E., Doi M., Shimasaku K., Schneider D. P., 1996, AJ, 111, 1748
 Gunn J. E., et al., 1998, AJ, 116, 3040
 Gunn J. E., et al., 2006, AJ, 131, 2332
 Hogg D. W., Finkbeiner D. P., Schlegel D. J., Gunn J. E., 2001, AJ, 122, 2129
 Ivezić Ž., et al., 2004, Astronomische Nachrichten, 325, 583
 Kozłowski S., et al., 2010, ApJ, 716, 530
 Kozłowski S., Kochanek C. S., Ashby M. L. N., Assef R. J., Brodwin M., Eisenhardt P. R., Jannuzi B. T., Stern D., 2016, ApJ, 817, 119
 Lacy M., et al., 2004, ApJS, 154, 166
 Lang D., 2014, AJ, 147, 108
 Lang D., Hogg D. W., Schlegel D. J., 2016, AJ, 151, 36
 Lupton R., Gunn J. E., Ivezić Ž., Knapp G. R., Kent S., 2001, in F. R. Harnden Jr., F. A. Primini, & H. E. Payne ed., Astronomical Data Analysis Software and Systems X Vol. 238 of Astronomical Society of the Pacific Conference Series, The SDSS Imaging Pipelines, p. 269
 Mainzer A., et al., 2014, ApJ, 792, 30
 Martínez-Sansigre A., Rawlings S., Lacy M., Fadda D., Jarvis M. J., Marleau F. R., Simpson C., Willott C. J., 2006, MNRAS, 370, 1479

- McAlpine S., Bower R. G., Harrison C. M., Crain R. A., Schaller M., Schaye J., Theuns T., 2017, ArXiv e-prints
 Meisner A. M., Lang D., Schlegel D. J., 2016, ArXiv e-prints
 Netzer H., 2015, ARA&A, 53, 365
 Oke J. B., Gunn J. E., 1983, ApJ, 266, 713
 Padmanabhan N., et al., 2008, ApJ, 674, 1217
 Páris I., Petitjean P., Ross N. P., et al., 2017, Astron. & Astrophys., 597, A79
 Pier J. R., Munn J. A., Hindsley R. B., Hennessy G. S., Kent S. M., Lupton R. H., Ivezić Ž., 2003, AJ, 125, 1559
 Pillepich A., et al., 2017, ArXiv e-prints
 Richards G. T., et al., 2002, AJ, 123, 2945
 Richards G. T., et al., 2009, AJ, 137, 3884
 Richards G. T., et al., 2015, ApJS, 219, 39
 Rosas-Guevara Y., Bower R. G., Schaye J., McAlpine S., Dalla Vecchia C., Frenk C. S., Schaller M., Theuns T., 2016, MNRAS, 462, 190
 Ross N. P., et al., 2012, ApJS, 199, 3
 Schneider D. P., et al., 2010, AJ, 139, 2360
 SDSS Collaboration Albareti F. D., Allende Prieto C., Almeida A., Anders F., Anderson S., Andrews B. H., Aragon-Salamanca A., Argudo-Fernandez M., Armengaud E., et al. 2016, ArXiv e-prints
 Shen Y., et al., 2011, ApJS, 194, 45
 Smith J. A., et al., 2002, AJ, 123, 2121
 Stern D., et al., 2005, ApJ, 631, 163
 Stern D., et al., 2012, ApJ, 753, 30
 Stoughton C., et al., 2002a, AJ, 123, 485
 Stoughton C., et al., 2002b, AJ, 123, 485
 Timlin J. D., et al., 2016, ApJS, 225, 1
 Tucker D. L., et al., 2006, Astronomische Nachrichten, 327, 821
 Wright E. L., et al., 2010, AJ, 140, 1868
 York D. G., et al., 2000, AJ, 120, 1579